Joint Channel and Frequency Offset Estimation for Oversampled Perfect Reconstruction Filter Bank Transceivers

Siavash Rahimi, *Student Member, IEEE*, and Benoit Champagne, *Senior Member, IEEE*

***Abstract*—Recently, DFT-based oversampled perfect reconstruction filter banks (OPRFB), as a special form of filtered multitone, have shown great promises for applications to multicarrier modulation. Still, accurate frequency synchronization and channel equalization are needed for their reliable operation in practical scenarios. In this paper, we first derive a data-aided joint maximum likelihood (ML) estimator of the carrier frequency offset (CFO) and the channel impulse response (CIR) for OPRFB transceiver systems operating over frequency selective fading channels. Then, by exploiting the structural and spectral properties of these systems, we are able to considerably reduce the complexity of the proposed estimator through simplifications of the underlying likelihood function. The Cramer Rao bound on the variance of unbiased CFO and CIR estimators is also derived. The performance of the proposed ML estimator is investigated by means of numerical simulations under realistic conditions with CFO and frequency selective fading channels. The effects of different pilot schemes on the estimation performance for applications over time-invariant and mobile time-varying channels are also examined. The results show that the proposed joint ML estimator exhibits an excellent performance, where it can accurately estimate the unknown CFO and CIR parameters for the various experimental setups under consideration.**

***Index Terms*—Data-aided estimation, channel impulse response, carrier frequency offset, maximum likelihood (ML), oversampled filter bank transceiver, CRB, multicarrier modulation.**

I. Introduction

DUE to its appealing features, multicarrier modulation (MCM) is recognized as the method of choice for high data rate wireless transmission. Orthogonal frequency division multiplexing (OFDM), the most common form of MCM, is used in many current and emerging standards [1], [2]. However, due to its implicit use of rectangular time-domain narrowband filters (with high sidelobe levels at -13 dB), OFDM exhibits a poor spectral containment and is therefore sensitive to frequency synchronization errors and narrowband interference. To overcome such limitations of OFDM, more general forms of MCM, referred to as filter bank multicarrier (FBMC), have been introduced that include OFDM/OQAM [3], filtered multitone (FMT) [4] and specializations thereof, such as the recently proposed oversampled perfect reconstruction filter banks (OPRFB) [5]–[8]. In FBMC systems, data symbols are transmitted over frequency adjacent subbands after some band-limited pulse shaping. Reduced sensitivity to narrowband interference, better spectral containment, and more flexibility in the multi-user scenarios are some of the advantages of FBMC systems [9], [10]. These appealing features have attracted considerable attention recently for emerging applications in wireless communications (e.g., digital video broadcasting [11] and cognitive radio [12]) and wireline transmissions (e.g., power line communication [13]).

The performance of FBMC systems in data transmission over frequency selective channels is studied in [14]–[16] for different prototype filters. It is generally shown that FBMC systems can outperform OFDM by a sizeable margin under non-ideal conditions of operation due to the better spectral containment of their subband filters. Nevertheless, they remain sensitive to the time and frequency selectivity of the channel and require accurate estimation of the channel impulse response (CIR) to combat these impairments through equalization. Moreover, similar to other types of MCM, FBMC systems are more sensitive to carrier frequency offset (CFO) than single carrier (SC) systems, since the CFO induced by the mismatch between the transmitter and receiver oscillators may result in intersymbol interference (ISI) or intercarrier interference (ICI) [17]–[22]. As a result, it is of particular interest to develop efficient CFO and CIR estimation techniques in order to compensate these channel impairments in FBMC systems.

In the past, a vast body of literature has been devoted to the study of CFO and CIR estimation algorithms for OFDM systems by relying on training sequence [23], cyclic prefix [24], iterative maximum likelihood (ML) [25] and expectation-maximization [26]. However, the consideration of these problems in the more general context of FBMC is fairly recent. CFO estimation for OFDM/OQAM systems is addressed in [16], [27], and[28] and the CIR estimation for these systems is reviewed in [29]. In particular, joint synchronization methods based on scattered pilots and the conjugate symmetry property of OFDM/OQAM are presented in [16], [28], [30], and[31]. One of the main efforts to jointly estimate the CFO and CIR for

Manuscript received September 4, 2013; revised January 24, 2014 and April 9, 2014; accepted April 11, 2014. Date of publication April 18, 2014; date of current version June 18, 2014. This work was supported in part by InterDigital Canada Ltée., by the Natural Sciences and Engineering Research Council of Canada, and by the Government of Québec under the PROMPT program. The associate editor coordinating the review of this paper and approving it for publication was H. Steendam.

The authors are with the Department of Electrical and Computer Engineering, McGill University, Montreal, QC H3A 0E9, Canada (e-mail: siavash.rahimi@mail.mcgill.ca; benoit.champagne@mcgill.ca).

Color versions of one or more of the figures in this paper are available online at http://ieeexplore.ieee.org.

Digital Object Identifier 10.1109/TCOMM.2014.2318717

critically sampled FMT systems is developed in [32], where the CIR is estimated in the frequency domain after CFO estimation in the time-domain. Several methods have also been proposed to mitigate the sensitivity of FBMC systems to synchronization errors assuming known or simplified CIR. A time-domain data-aided symbol timing and CFO synchronization method based on the least square (LS) approach is developed in [27] for FMT and OFDM/OQAM systems operating over frequency-flat additive white Gaussian noise (AWGN) channel. Alternatively, in [33] and [34], the authors propose a frequency-domain ML-based data-aided CFO estimation algorithm for FMT systems. The results in these works show that the data-aided methods outperform the blind ones (i.e., non-data-aided) proposed in [35] and[36] in terms of estimation accuracy and complexity.

Among the various approaches reported in the recent literature for the design and implementation of FBMC systems, those based on discrete Fourier transform (DFT) modulation, such as OFDM/OQAM and OPRFB are particularly appealing as they exhibit outstanding performance in wireless scenarios. Within this class, OFDM/OQAM has received considerable attention, especially under the auspices of the PHYDYAS project in Europe [37]. Nevertheless, it poses a number of practical difficulties, as the real and imaginary parts of the complex-valued QAM symbols from adjacent subbands must be staggered in time by half a symbol. This requires the use of additional pre/post-processing modules at the transmit/receive sides to extract and offset the real and imaginary parts. These modifications add to the system complexity and make the implementation of multiple-input multiple-output (MIMO) coding schemes nontrivial [9]. In addition, the overlapping of adjacent subbands may induce significant ICI when transmission is over a non-ideal channel. Therefore, equalization both across time and frequency may be required.

In contrast, OPRFB does not employ these extra modules and can be easily applied to MIMO coding schemes since complex orthogonality is intrinsically provided and its equalization is simpler. In effect, OPRFB can be viewed as a specific form of FMT where the perfect reconstruction (PR) property is enforced by employing oversampled filter banks. This constraint can facilitate the equalization process and brings desirable spectral containment (albeit at the cost of longer filters which may increase latency and complexity to some extent). Moreover, at high SNR, a PR system can generally achieve a lower bit error rate (BER) compared to a non-PR one, which introduces an undesirable lower floor on the achievable BER [8]. These reasons motivate the consideration of OPRFB systems for FBMC applications in this work.

While the aforementioned contributions to the estimation of CFO and CIR in the context of FBMC systems are valuable, they cannot be directly applied to OPRFB due to intrinsic structural differences in signal and filter formats. For instance, the essential assumption in the method proposed in [33] and [34], i.e., constant CFO effect over the duration of the receive filters, is not valid for OPRFB systems as they employ relatively longer prototype filters. In addition, a majority of these works are based on an oversimplified broadband flat fading channel model, where the CIR reduces to a single coefficient [27], [35], [36], [38]. It was just recently that the authors proposed a CFO estimation method targeted for OPRFB systems [38]; however, it assume perfect knowledge of the CIR in the equalization process and therefore does not qualify as a joint estimation technique. Hence, despite its importance, the study of advanced CFO and CIR compensation schemes for OPRFB remains largely unexplored.

In this paper, we first develop a data-aided joint ML estimator of the CFO and CIR that is specifically designed for OPRFB systems, but also applicable to FMT systems, operating over frequency selective fading channels. Then, by exploiting the structural and spectral properties of these systems, we are able to considerably reduce the complexity of the proposed estimator through simplifications of the underlying likelihood function. The Cramer Rao bound (CRB) on the variance of joint unbiased CFO and CIR estimators is also derived as a by-product of the ML analysis. The performance of the proposed joint ML estimator is investigated by means of simulations under realistic conditions of transmission with CFO and frequency selective fading channels. The effects of using different pilot schemes for applications in wireless scenarios over time-invariant and mobile time-varying channels are also examined. The results show that the proposed joint ML estimator exhibits an excellent performance, where it can accurately estimate the unknown CFO and CIR parameters for the various experimental setups under consideration. Using these estimates, it is possible to compensate the effects of CFO and frequency selective fading channel on the transmission performance of OPRFB-based MCM systems under realistic wireless conditions. Finally, by employing different pilot patterns, we show that in mobile scenarios with fast time-varying channels, the proposed joint estimator and compensation methods still exhibit a reliable performance.

The rest of the paper is organized as follows. Section II presents the OPRFB system model and discusses the effects of CFO on the signal recovery process at the receiver side. The joint ML estimator of the CFO and CIR is developed in Section III, along with relevant practical simplifications, while the CRB on the joint estimator variance is derived in Section IV. The performance of the proposed joint estimator is evaluated in Section V and some conclusions are offered in Section VI. Notation: $\jmath = \sqrt{-1}$. Bold-faced letters indicate vectors and matrices, e.g., $\mathbf{A}$. The (i,j)th entry of a matrix is represented by $[\mathbf{A}]_{i,j}$. The superscripts T and H stand for the transpose and Hermitian transpose of a vector or matrix, respectively, while the superscript $*$ denotes complex conjugation. $\mathbf{I}$ and $\mathbf{0}$, respectively denote the identity and zero matrices. The paraconjugate operation on a matrix function $\mathbf{E}(z)$ is defined by $\tilde{\mathbf{E}}(z) = \mathbf{E}(1/z^*)^H$. $E\{.\}$, $\mathsf{Re}[.]$ and $\mathsf{Im}[.]$ stand for the expected value, real part and imaginary part of their arguments, respectively.

II. Problem Formulation

In this section, the OPRFB system model is presented along with its input-output relation over a frequency selective fading channel. The effects of the CFO on the reconstructed signal are discussed and finally, the joint estimation problem for the CFO and CIR is stated.

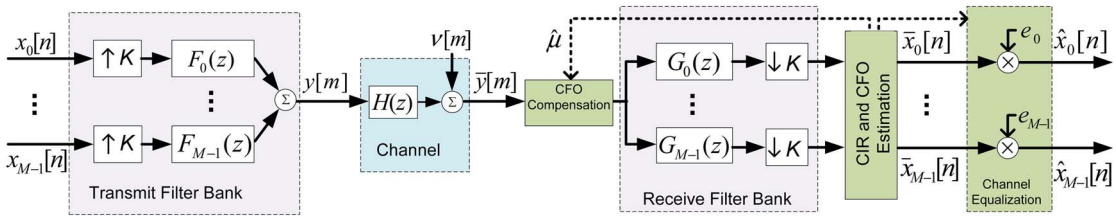

Fig. 1. DFT-modulated OPRFB transceiver with CFO and CIR estimation.

A. OPRFB System Model

We consider a DFT-modulated OPRFB transceiver system, as depicted in Fig. 1. Parameters M and K represent the number of subbands and the upsampling/downsampling factor, respectively, where $K > M$ (oversampling) is assumed [8]. In DFT-modulated FBMC systems, the transmit and receive subband filters can be derived from common prototypes with finite impulse responses (FIR) of length D and respective system functions $F_0(z) = \sum_{n=0}^{D-1} f_0[n]z^{-n}$ and $G_0(z) = \sum_{n=0}^{D-1} g_0[n]z^{n}$, where $f_0[n]$ and $g_0[n]$ are the corresponding impulse response coefficients. For convenience in analysis, $G_i(z)$ is assumed non-causal although in practice, causality can be restored simply by introducing an appropriate delay in the receiver. Defining $w = e^{-\jmath 2\pi/M}$, the DFT-modulated transmit and receive filters for the ith subband are respectively obtained as

$$F_i(z) = F_0(zw^i), \quad G_i(z) = G_0(zw^i). \tag{1}$$

In this paper, the filter length D is restricted to be a multiple of M and K, i.e., $D = d_P P$, where P denotes the least common multiple of M and K and d_P is a positive integer. To enforce the PR property, the paraconjugates of the transmit filters are employed as receive filters, i.e., $g_i[n] = f_i^*[n]$. Under this setting, PR can be expressed as

$$\sum_{q=-\infty}^{\infty} f_j[q - pK] f_i^*[q - nK] = \delta_{ij}\delta_{np} \tag{2}$$

where δ_{ij} denotes the Kronecker delta function.

Let $x_i[n]$ denote the complex-valued data symbol transmitted on the ith subband at discrete-time nT_s, where $i \in \{0, \ldots, M-1\}$, $n \in \mathbb{Z}$, $T_s = F_s^{-1}$ and F_s is the input sampling rate. On the transmitter side, as shown in Fig. 1, the input sequences $x_i[n]$ are upsampled by K, passed through their corresponding subband filter $F_i(z)$, and finally summed. Hence, the transmitter output signal at discrete-time mT_s/K is given by

$$y[m] = \sum_{i=0}^{M-1} \sum_{q=-\infty}^{\infty} x_i[q] f_i[m - qK] \tag{3}$$

where the range of the summation over q is delimited by the finite support of the subband FIR filter, $f_i[m]$.

In a practical system implementation, the signal $y[m]$ is upconverted to a suitable frequency band via carrier frequency modulation and then transmitted over a noisy channel, while at the receiver, the reverse demodulation operations are applied. Here, we consider a baseband equivalent model of these operations in terms of the signal samples $y[m]$.

We assume that during a time interval equal to the processing delay of the transceiver system (i.e., $2DT_s/K$), the transmission channel can be modeled as a linear time-invariant system with FIR $h[l]$ of length Q and corresponding system function $H(z) = \sum_{l=0}^{Q-1} h[l]z^{-l}$. In this model, the filter length Q is chosen according to the multipath delay spread τ_{ds} of the channel, i.e., $QT_s = K\tau_{ds}$. The channel output is corrupted by an AWGN sequence $\nu[m]$, with zero-mean and variance $E[|\nu[m]|^2] = \sigma_\nu^2$, assumed to be statistically independent from the input data. The input-output relationship of the noisy channel can therefore be expressed as

$$\bar{y}[m] = \sum_{l=0}^{Q-1} h[l] y[m - l] + \nu[m] \tag{4}$$

where $\bar{y}[m]$ denotes the received baseband discrete-time signal. On the receiver side, $\bar{y}[m]$ is passed through a bank of M analysis filters and downsampled by K. Accordingly, for each subband, the reconstructed signal $\bar{x}_i[n]$ can be written as

$$\bar{x}_i[n] = \sum_{q=-\infty}^{\infty} \bar{y}[q] f_i^*[q - nK]. \tag{5}$$

Note that in the case of an ideal channel with no noise (i.e., $H(z) = 1$ and $\nu[m] = 0$), the PR condition (2) ensures that $\bar{x}_i[n] = x_i[n]$, $\forall\, i, n$.

B. Effects of Carrier Frequency Offset

In practice, there often exists a mismatch between the carrier frequency in the receiver and the transmitter, denoted as CFO. In this case, the received signal $\bar{y}[m]$ can be modeled as [27], [39]

$$\bar{y}[m] = e^{\jmath 2\pi \frac{\mu}{M} m} \sum_{l=0}^{Q-1} h[l] y[m - l] + \nu[m] \tag{6}$$

where μ is a normalized CFO with respect to the subband spacing $F_s K/M$. Here, we assumed that there is no time offset between the transmitter and receiver or it is estimated and compensated by other means.

Upon substitution of (6) and then (3) into (5), the reconstructed signal for the ith subband, $\bar{x}_i[n]$, can be written in terms of the input signals $x_j[n]$, for $j \in \{0, \ldots, M-1\}$, as

$$\bar{x}_i[n] = \sum_{l=0}^{Q-1} \lambda_{i,n}(l, \mu) h[l] + \nu_i[n] \tag{7}$$

where $\lambda_{i,n}(l,\mu)$ and $\nu_i[n]$ are defined as

$$\lambda_{i,n}(l,\mu) = \sum_{j=0}^{M-1} \sum_{p=-\infty}^{\infty} x_j[p]\gamma_{i,n}^{j,p}(l,\mu) \tag{8}$$

$$\gamma_{i,n}^{j,p}(l,\mu) = \sum_{q=-\infty}^{\infty} e^{\jmath 2\pi \frac{\mu}{M} q} f_j[q-l-pK] f_i^*[q-nK] \tag{9}$$

$$\nu_i[n] = \sum_{q=-\infty}^{\infty} \nu[q] f_i^*[q-nK]. \tag{10}$$

As can be seen from (7) and (8) by temporarily omitting the noise term $\nu_i[n]$, the complex factor $\gamma_{i,n}^{j,p}(l,\mu)$ in (9) characterizes the interference level of the pth input sample from the jth subband, that is $x_j[p]$, on the nth output sample of the ith subband, $x_i[n]$, in the presence of CFO with magnitude μ through the lth path of the radio channel $h[l]$. We note that for $|n-p| > (D+Q)/K$, due to the finite support of the subband filters $f_i[n]$, $\gamma_{i,n}^{j,p}(l,\mu) = 0$; accordingly, the range of the summation over p in (8) is indeed finite. The term $\nu_i[n]$ (10) represents the additive noise passed through the ith subband of the receive filter bank. This term has zero-mean and, due to the PR property imposed on $f_i[n]$ in (2), its covariance (as derived in the Appendix A) is given by

$$E\left\{\nu_i[p]\nu_j^*[q]\right\} = \delta_{ij}\delta_{pq}\sigma_\nu^2. \tag{11}$$

Considering the reconstructed signal $\bar{x}_i[n]$ in (7), it appears that even if the channel could be perfectly equalized (equivalent to $h[0]=1$ and $h[l]=0$ for $l \neq 0$) the presence of the CFO term $e^{\jmath 2\pi(\mu/M)q}$ in the interference factor, $\gamma_{i,n}^{j,p}(l,\mu)$(9) would render the transceiver system non-PR. That is, $\gamma_{i,n}^{j,p}(l,\mu)$ would be non-zero for $j \neq i$ or $p \neq n$, and this in turn would result in a loss of performance in the data transmission process. It is worth to mention that in previous works [33], [34], it is assumed that since the finite support of $f_i[n]$ and the CFO value μ are often small, the exponential CFO term $e^{\jmath 2\pi(\mu/M)q}$ remains constant. If this was the case, this term could be taken out of the summation over q in (9) and, consequently, the interference terms $\gamma_{i,n}^{j,p}(l,\mu)x_j[p]$ would be negligible when $j \neq i$ or $p \neq n$. This oversimplification may function for some situations in FMT systems, however, it does not hold for OPRFB systems as they employ relatively longer prototype filters.

C. Problem Formulation

As seen from Fig. 1, if a suitable estimate of μ is available, say $\hat{\mu}$, it can be used to compensate the CFO at the receiver front-end and thereby avoid its deleterious effects. Similarly, if estimates of the CIR coefficients $h[l]$ are available, denoted as $\hat{h}[l]$ for $l \in \{0,\ldots,Q-1\}$, they can be used on the receiver side to design a set of subband equalizers to counteract the distortion incurred by the input signals during their transmission. In this paper, we focus on single-tap per subcarrier equalizer, as represented by the coefficients e_i in Fig. 1, where $i \in \{0,\cdots M-1\}$, but generalizations to other, more advanced types of equalizers are possible. This simple equalization scheme inverts the channel at the center frequency of the corresponding subcarrier and it works well in mildly selective channels as long as the number of subcarriers is sufficiently large [40].

Our interest in this work, therefore, lies in the development of an efficient, data-aided ML based approach for the joint estimation of the CFO parameter μ and CIR coefficients $\{h[l]\}_{l=0}^{Q-1}$. We favor the use of data-aided over blind estimation, since the latter generally requires a long data record to achieve a desired level of accuracy, which in turns entails high computational complexity and limits applications to static or slowly time-varying channels. We consider the framework of point estimation theory, where the parameters under estimation are modeled as unknown, yet deterministic quantities, i.e., no prior distribution is assumed. Given the transmission of a known sequence of pilots, and the subsequent observation of the reconstructed subband signals over a given time interval, our aim is to develop and investigate the properties of the joint ML estimator of μ and $\{h[l]\}$.

III. Joint Estimation

In this section, we first derive a joint estimator of the CFO and CIR based on the ML principle, which employs known transmitted pilot symbols. We then propose a number of practical simplifications in the calculation of the associated log-likelihood function (LLF) that result in a lower implementation complexity for this estimator.

A. Data-Aided ML Estimator

We define a multi-carrier symbol (MCS)[1] as the ordered set of M subband inputs $x_i[n]$, for $i \in \{0,1,\ldots,M-1\}$, entering the transmit filter bank at time n. We assume that within a burst of N consecutive MCS, say from time $n=0$ to $N-1$, a total of T MCS with time indices in $\mathcal{T} = \{t_n | 0 \leq t_0 < t_1 < \cdots < t_{T-1} \leq N-1\}$, referred to as pilot-times, are selected for the transmission of pilots over selected subbands. At any given time t_n, a subset of S subbands with frequency indices in $\mathcal{S} = \{s_i | 0 \leq s_0 < s_1 \cdots, < s_{S-1} \leq M-1\}$, referred to as pilot-subbands, are dedicated to the transmission of pilot symbols $\mathsf{p}_{s_i}[t_n]$. In effect, we consider a rectangular lattice of $N_P = TS$ pilot symbols distributed over the time-frequency plane. Note that N_P should be greater than Q to guarantee that there exists enough data to estimate the $Q+1$ unknown CFO and CIR parameters, i.e., μ and $\mathbf{h}$. Given the limited amount of training data that can be sent to estimate these parameters, it is prudent to select $\mathcal{S}$ and $\mathcal{T}$ such that the resulting estimates achieve a good performance (if not optimal) among other possible choices of $\mathcal{S}$ and $\mathcal{T}$ with the same N_P.

In that regard, we consider two main schemes for the distribution of the pilot symbols over the frequency axis, i.e., choices of the index set $\mathcal{S}$. In the first one, labeled as Scheme A for convenience, the pilot-subbands occupy adjacent positions along the frequency axis, i.e., $s_i - s_{i-1} = 1$. In the second one labeled as Scheme B, the pilot-subbands are equispaced to evenly cover the frequency axis, i.e., $s_i - s_{i-1} = \lfloor M/S \rfloor$, where $\lfloor . \rfloor$ denotes the floor function. Obviously, these two schemes are equivalent when $S = M$. Similarly, in terms of

[1]This is also called a vector symbol in the MCM literature.

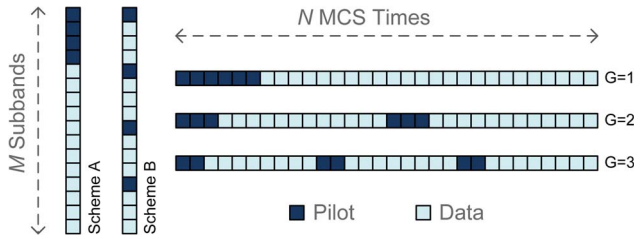

Fig. 2. Distribution of pilots over frequency (Scheme A and Scheme B with $S = 4$ pilot-subbands in $M = 16$ subbands) and time ($G = 1, 2,$ and 3 groups for $T = 6$ pilot-times in a burst of $N = 30$ MCS).

the distribution of pilot symbols over time, the index set $\mathcal{T}$ can be chosen in different ways. Here, we consider a scheme in which the T pilot-times are divided into G groups evenly distributed throughout a burst, with each group consisting of T/G consecutive MCS, where we assume T/G is an integer for simplicity. Examples of the distributions of pilot symbols over the frequency and time axes are depicted in Fig. 2.

Let $z_{s_i}[t_n]$ denote the reconstructed signal corresponding to the transmitted pilot $\mathsf{p}_{s_i}[t_n]$. From (7), it follows that:

$$\begin{aligned} z_{s_i}[t_n] &= \sum_{l=0}^{Q-1} \lambda_{s_i,t_n}(l,\mu)h[l] + \nu_{s_i}[t_n] \\ &= \sum_{l=0}^{Q-1} \bar{\lambda}_{s_i,t_n}(l,\mu)h[l] + w_{s_i}[t_n] + \nu_{s_i}[t_n] \end{aligned} \quad (12)$$

where $\bar{\lambda}_{s_i,t_n}(l,\mu)$ and $w_{s_i}[t_n]$ are defined as

$$\bar{\lambda}_{s_i,t_n}(l,\mu) = \sum_{j\in\mathcal{S}} \sum_{p\in\mathcal{T}} \mathsf{p}_j[p]\gamma^{j,p}_{s_i,t_n}(l,\mu) \quad (13)$$

$$w_{s_i}[t_n] = \sum_{l=0}^{Q-1} \sum_{j\notin\mathcal{S}} \sum_{p\notin\mathcal{T}} x_j[p]\gamma^{j,p}_{s_i,t_n}(l,\mu)h[l]. \quad (14)$$

Moreover, the term $\bar{\lambda}_{s_i,t_n}(l,\mu)$ in (13) conveys the same physical meaning for the pilot symbols, as does the term $\lambda_{i,n}(l,\mu)$ in (8) for the input symbols. Specifically, it represents the contribution from all the pilot-symbols, as represented by the set of $\{\mathsf{p}_j[p] : j \in \mathcal{S}, p \in \mathcal{T}\}$, to the output $z_{s_i}[t_n]$, through the lth channel path. In contrast, $w_{s_i}[t_n]$ (14) represents the total contribution from the non-pilot (i.e., data carrying) input symbols to $z_{s_i}[t_n]$ and can therefore be interpreted as a form of *data-interference* in the estimation process. Considering the input symbols $x_j[p]$ as independent and identically distributed random variables with zero-mean and variance σ_x^2, it is shown in the Appendix B that these interference terms $w_{s_i}[t_n]$ can be approximated as independent Gaussian random variables with zero-mean and variance

$$\sigma_w^2 = E\left\{|w_{s_i}[t_n]|^2\right\} = \sigma_x^2 \sum_{j\notin\mathcal{S}} \sum_{p\notin\mathcal{T}} \left|\Gamma^{j,p}_{s_i,t_n}(\mu)\right|^2 \quad (15)$$

where $\Gamma^{j,p}_{s_i,t_n}(\mu) = \sum_{l=0}^{Q-1} \gamma^{j,p}_{s_i,t_n}(l,\mu)h[l]$. Introducing $v_{s_i}[t_n] = w_{s_i}[t_n] + \nu_{s_i}[t_n]$, (12) can be rewritten as

$$z_{s_i}[t_n] = \sum_{l=0}^{Q-1} \bar{\lambda}_{s_i,t_n}(l,\mu)h[l] + v_{s_i}[t_n]. \quad (16)$$

If we further assume that the data symbols $x_j[p]$ and additive noise $\nu_{s_i}[t_n]$ are independent, it follows that $v_{s_i}[t_n]$ are independent Gaussian random variables with zero-mean and variance $\sigma_v^2 = \sigma_w^2 + \sigma_\nu^2$.

For convenience, we let $\mathbf{h} = [h[0], h[1], \ldots, h[Q-1]]^T$ denote the column vector of unknown channel coefficients and define the row vector

$$\boldsymbol{\lambda}_{s_i,t_n}(\mu) = \left[\bar{\lambda}_{s_i,t_n}(0,\mu), \bar{\lambda}_{s_i,t_n}(1,\mu), \ldots, \bar{\lambda}_{s_i,t_n}(Q-1,\mu)\right]. \quad (17)$$

In terms of these, (16) can be expressed as

$$z_{s_i}[t_n] = \boldsymbol{\lambda}_{s_i,t_n}(\mu)\mathbf{h} + v_{s_i}[t_n]. \quad (18)$$

In order to express the set of (18) in compact vector form, we first introduce

$$\mathbf{z}_{s_i} = [z_{s_i}[t_0], z_{s_i}[t_1], \ldots, z_{s_i}[t_{T-1}]]^T \quad (19)$$

$$\boldsymbol{\lambda}_{s_i}(\mu) = \left[\boldsymbol{\lambda}_{s_i,t_0}(\mu)^T, \boldsymbol{\lambda}_{s_i,t_1}(\mu)^T, \ldots, \boldsymbol{\lambda}_{s_i,t_{T-1}}(\mu)^T\right]^T \quad (20)$$

$$\mathbf{v}_{s_i} = [v_{s_i}[t_0], v_{s_i}[t_1], \ldots, v_{s_i}[t_{T-1}]]^T. \quad (21)$$

From (18), we have

$$\mathbf{z}_{s_i} = \boldsymbol{\lambda}_{s_i}(\mu)\mathbf{h} + \boldsymbol{v}_{s_i}. \quad (22)$$

We then stack these vectors and matrices over the frequency, and define

$$\mathbf{Z} = \left[\mathbf{z}_{s_0}^T, \mathbf{z}_{s_1}^T, \ldots, \mathbf{z}_{s_{S-1}}^T\right]^T \quad (23)$$

$$\boldsymbol{\Lambda}(\mu) = \left[\boldsymbol{\lambda}_{s_0}(\mu)^T, \boldsymbol{\lambda}_{s_1}(\mu)^T, \ldots, \boldsymbol{\lambda}_{s_{S-1}}(\mu)^T\right]^T \quad (24)$$

$$\mathbf{V} = \left[\mathbf{v}_{s_0}^T, \mathbf{v}_{s_1}^T, \ldots, \mathbf{v}_{s_{S-1}}^T\right]^T \quad (25)$$

so that

$$\mathbf{Z} = \boldsymbol{\Lambda}(\mu)\mathbf{h} + \mathbf{V} \quad (26)$$

where $\boldsymbol{\Lambda}(\mu)$ is an $N_P \times Q$ matrix, assumed to be of full column rank.[2]

As a consequence of the AWGN model assumption and subsequent approximations on the data-interference $w_{s_i}[t_n]$, it follows that $\mathbf{V}$ is a complex circular Gaussian random vector with zero-mean and diagonal covariance matrix $\mathbf{C}_\mathbf{V} = E[\mathbf{V}\mathbf{V}^H] = \sigma_v^2\mathbf{I}$. Accordingly, for given values of the unknown parameters μ and $\mathbf{h}$, the observation vector $\mathbf{Z}$ in (26) is also complex circular Gaussian with mean $\boldsymbol{\Lambda}(\mu)\mathbf{h}$ and covariance $\mathbf{C}_Z = \sigma_v^2\mathbf{I}$. The probability density function (PDF) of $\mathbf{Z}$, say $f(\mathbf{Z};\mu,\mathbf{h})$ can therefore be formulated as

$$\begin{aligned} f(Z;\mu,\mathbf{h}) &= \frac{1}{\pi^{N_P}\det(\mathbf{C}_Z)} \\ &\quad \cdot \exp\left[-\left(\mathbf{Z} - \boldsymbol{\Lambda}(\mu)\mathbf{h}\right)^H \mathbf{C}_Z^{-1}\left(\mathbf{Z} - \boldsymbol{\Lambda}(\mu)\mathbf{h}\right)\right]. \end{aligned} \quad (27)$$

[2]This assumption was observed to be satisfied in all of our experiments over several different setup configurations.

Taking the natural logarithm of this PDF, the LLF [41] for the parameters μ and $\mathbf{h}$ can be expressed (up to a constant term) in the form

$$\mathcal{L}(\mathbf{Z};\mu,\mathbf{h}) = \log\left(f(\mathbf{Z}|\mu,\mathbf{h})\right) = -\frac{1}{\sigma_v^2}\left[\mathbf{Z}-\mathbf{\Lambda}(\mu)\mathbf{h}\right]^H\left[\mathbf{Z}-\mathbf{\Lambda}(\mu)\mathbf{h}\right]. \quad (28)$$

The joint ML estimators of the CFO and CIR is obtained by maximizing the LLF (28) with respect to the unknown parameters μ and $\mathbf{h}$. In effect, this maximization amounts to finding the hypothetical values of the CFO and CIR such that the distorted pilots by these parameter values best match (in the LS sense) the reconstructed pilots at the output of the receive filter bank.

Since the LLF (28) is quadratic in the CIR parameters, a closed-form solution can be obtained for the optimum $\mathbf{h}$ in terms of μ. Specifically, fixing μ and varying $\mathbf{h}$ in $\mathbb{C}^Q$, the LLF (28) achieves its maximum at

$$\mathbf{h}_o(\mu) = \mathbf{\Lambda}(\mu)^\dagger\mathbf{Z} \quad (29)$$

where $\mathbf{\Lambda}(\mu)^\dagger = \left(\mathbf{\Lambda}(\mu)^H\mathbf{\Lambda}(\mu)\right)^{-1}\mathbf{\Lambda}(\mu)^H$ is the pseudo-inverse of $\mathbf{\Lambda}(\mu)$. Next, upon substitution of (29) in (28), the ML estimate of the CFO can be obtained via a 1-D search, i.e.,

$$\hat{\mu} = \arg\max_{\mu\in\mathcal{M}}\left\{\mathcal{L}\left(\mathbf{Z};\mu,\mathbf{h}_o(\mu)\right)\right\} \quad (30)$$

where $\mathcal{M}$ is the search range for μ. In practice, the optimization problem (30) can be solved in two stages. The first stage, or coarse search, computes $\mathcal{L}(\mathbf{Z};\mu,\mathbf{h}_o(\mu))$ over a uniform grid of μ values and determines the location of its maximum on the grid, say μ_m. The second stage, or fine search, attempts to find the local maximum nearest to μ_m, which can be handled by classic optimization methods due to the observed convexity of the LLF $\mathcal{L}(\mathbf{Z};\mu,\mathbf{h}_o(\mu))$ in the vicinity of the true CFO. Since this LLF is periodic in μ with a period of one subband spacing for various pilot distributions, the search range $\mathcal{M}$ must be less than half the subband spacing to avoid ambiguity in the estimation. Finally, the ML estimate of the CIR is obtained by substituting the $\hat{\mu}$ in (29), that is

$$\hat{\mathbf{h}} = \mathbf{h}_o(\hat{\mu}) = \mathbf{\Lambda}(\hat{\mu})^\dagger\mathbf{Z}. \quad (31)$$

Except for Q, the maximum delay spread,[3] no *a priori* information about the channel is required to implement the above ML estimator of the CFO and CIR. We also note that since the CFO μ is estimated first based on (30) and then exploited to obtain the CIR $\mathbf{h}$ via (31), this approach enables decoupling the estimation of the CFO from the CIR. Finally, for frequency-flat fading channels with $Q = 1$, the proposed method reduces to the ML CFO estimator previously reported by the authors in [38].

[3]The maximum delay spread, and therefore Q can be estimated using various methods such as the one reported in [42]. One might consider using a slightly larger value of Q for better reliability in case of possible error in the channel delay spread estimation, at the expense of higher complexity.

B. Simplifications of the LLF

Here, we propose two simplifications for $\bar{\lambda}_{s_i,t_n}(l,\mu)$ in (13), which considerably speed up the calculation of the LLF (30).

First consider the terms $\gamma^{j,p}_{s_i,t_n}(l,\mu)$ in (9), whose definition includes a summation over the length D (often large) of the prototype filter $f_0[q]$. Recalling that for DFT-modulated filter banks, we have $f_i[q] = f_0[q]w^{-iq}$, we can write

$$\gamma^{j,p}_{s_i,t_n}(l,\mu) = w^{jl+K(pj-s_it_n)}\varphi^{t_n,p}_{s_i-j}(l,\mu) \quad (32)$$

where

$$\varphi^{n,p}_\alpha(l,\mu) = \sum_{q=-\infty}^{\infty} e^{\jmath 2\pi\frac{\mu}{M}q} f_0[q-l-pK]f_0^*[q-nK]w^{q\alpha}. \quad (33)$$

By this simplification, instead of calculating $\gamma^{j,p}_{s_i,n}(l,\mu)$ for all the SM possible pairs (s_i,j), it is sufficient to compute $\varphi^{n,p}_\alpha(l,\mu)$ for only possible values of $s_i - j = \alpha$ and find the corresponding $\gamma^{j,p}_{s_i,t_n}(l,\mu)$ by multiplication with a discrete phase factor as in (32). The number of possible values of α depends on the distribution of the pilots over the frequency axis, where it is equal to $M+S-1$ and $2M - M/S$ for scheme A or B, respectively. Consequently, the number of operations needed to compute the terms $\gamma^{j,p}_{s_i,t_n}(l,\mu)$ is reduced by a factor of $SM/(M+S-1)$ for scheme A and $SM/(2M-M/S) \simeq S/2$ for scheme B.

Next, consider the $\bar{\lambda}_{s_i,t_n}(l,\mu)$ in (13). Due to the excellent spectral containment of the prototype filters, we can assume that the main source of the CFO-induced interference on each target subband is due to its first few neighboring subbands, and that interference from more distant subbands is negligible [38]. Therefore, as the second proposed simplification, to derive the total interference from subbands $j \in \mathcal{S}$ on the subband with index s_i in (13), it is sufficient to only factor in the contribution from a few neighboring pilot-carrying subbands on each side of the s_ith one. As a result, (13) is approximated as

$$\bar{\lambda}_{s_i,t_n}(l,\mu) \approx \sum_{j=i-\beta}^{i+\beta}\sum_{p\in\mathcal{T}} \mathsf{p}_j[p]\gamma^{s_j,p}_{s_i,t_n}(l,\mu) \quad (34)$$

where in practice, the value of β can be set to 2 for Scheme A or less for Scheme B. This allows a reduction in the number of required operations to compute $\bar{\lambda}_{s_i,t_n}(l,\mu)$ by a factor $S/(2\beta+1)$ as j will only take $2\beta+1$ values instead of all the possible S subband index values.

C. Complexity Evaluation

Thanks to the closed form CIR solution in (29), the multi-dimensional ML parameter estimation is reduced to the single-dimensional search of the LLF (28), more specifically $\mathcal{L}(\mathbf{Z};\mu,\mathbf{h}_o(\mu))$, over the unknown CFO parameter μ. This process is carried out in two stages, namely a coarse grid search (over about 20 points) leading to a preliminary estimate μ_m, followed by a fine search (typically between 5 to 20 points) around μ_m to obtain the final ML estimate $\hat{\mu}$. The second stage can be handled by classic optimization methods due to the observed convexity of the LLF in the vicinity of the

true CFO. Consequently, the main factor in determining the computational complexity of the proposed joint ML estimator is the number of operations required for each evaluation of the LLF $\mathcal{L}(\mathbf{Z};\mu,\mathbf{h}_o(\mu))$, as given by (28) and (29). Upon detailed inspection of these expressions, we find that this requires approximately $C \simeq 3DQN_P^2 + 4N_PQ^2 + (2/3)Q^3 + \mathcal{O}(N_PQ)$ complex-valued operations, where it can be seen that the first term is typically much larger than the others. This allows us to conclude that the overall complexity is proportional to the squared number of pilot symbols in the burst, which is consistent with the complexity analysis presented in [34] for a CFO-only ML-based estimator. The above evaluation of the complexity for the proposed joint ML approach corresponds to a worst case implementation where none of the simplifications presented in Section III-B are employed. When such simplifications are introduced, the leading coefficient of $3DQ$ in the first term of the above expression can be reduced significantly by a factor of $\sim M^2/(2+1)$.

Once suitable estimates of the CFO and CIR are available, they can be used to compensate the CFO at the receiver front-end as well as equalize the distortion incurred by the data signals during their transmission. This process, and consequently the computational complexity associated with it, is relatively similar to that of other FBMC methods.

IV. Joint Cramer Rao Bound

In this section, we derive the CRB on the covariance matrix of unbiased estimators of the CFO and CIR, assuming the transmitted signals are known (i.e., pilots). We let $\boldsymbol{\theta}$ denote the complete vector of unknown (real) parameters

$$\boldsymbol{\theta} = \left[\mu, \mathbf{h}_R^T, \mathbf{h}_I^T\right]^T \tag{35}$$

where $\mathbf{h}_R = \mathsf{Re}[\mathbf{h}] = [h_R[0], h_R[1], \ldots, h_R[Q-1]]^T$ and $\mathbf{h}_I = \mathsf{Im}[\mathbf{h}] = [h_I[0], h_I[1], \ldots, h_I[Q-1]]^T$ represent the real and imaginary parts of $\mathbf{h} = \mathbf{h}_R + \jmath\mathbf{h}_I$. Vector $\boldsymbol{\theta}$ consists therefore of $2Q+1$ real entries, which will be indexed by a or $b \in \{0,1,\ldots,2Q\}$. The order of the unknown parameters in this vector is similar to that of [43]. Let $\mathcal{I}(\boldsymbol{\theta})$ denote the $(2Q+1)\times(2Q+1)$ Fisher information matrix (FIM) for the estimation problem under consideration. Since $\partial\mathbf{C}_\mathbf{V}/\partial\theta_a = \mathbf{0}$ for $0 \le a \le 2Q$, the (a,b)th entry of $\mathcal{I}(\boldsymbol{\theta})$ is given by [41]

$$\begin{aligned}[\mathcal{I}(\boldsymbol{\theta})]_{a,b} &= E\left\{\frac{\partial^2\mathcal{L}(\mathbf{Z};\boldsymbol{\theta})}{\partial\theta_a\partial\theta_b}\right\} \\ &= 2\mathsf{Re}\left[\frac{\partial\left(\boldsymbol{\Lambda}(\mu)\mathbf{h}\right)^H}{\partial\theta_a}\mathbf{C}_Z^{-1}\frac{\partial\left(\boldsymbol{\Lambda}(\mu)\mathbf{h}\right)}{\partial\theta_b}\right] \\ &= \frac{2}{\sigma_v^2}\mathsf{Re}\left[\sum_{i=0}^{S-1}\sum_{n=0}^{L-1}\frac{\partial\left(\boldsymbol{\lambda}_{s_i,t_n}(\mu)\mathbf{h}\right)^*}{\partial\theta_a}\frac{\partial\left(\boldsymbol{\lambda}_{s_i,t_n}(\mu)\mathbf{h}\right)}{\partial\theta_b}\right].\end{aligned} \tag{36}$$

To evaluate the FIM, we consider the partial derivative of $\boldsymbol{\lambda}_{s_i,t_n}(\mu)\mathbf{h}$ with respect to θ_a for three different ranges of the index a, namely: $a=0$, $1 \le a \le Q$ and $Q+1 \le a \le 2Q$.

When $a = 0$, we have

$$\begin{aligned}\frac{\partial\left(\boldsymbol{\lambda}_{s_i,t_n}(\mu)\mathbf{h}\right)}{\partial\theta_0} &= \frac{\partial\left(\boldsymbol{\lambda}_{s_i,t_n}(\mu)\mathbf{h}\right)}{\partial\mu} \\ &= \frac{\partial\boldsymbol{\lambda}_{s_i,t_n}(\mu)}{\partial\mu}\mathbf{h}.\end{aligned} \tag{37}$$

For $1 \le a \le Q$, we can write

$$\begin{aligned}\frac{\partial\left(\boldsymbol{\lambda}_{s_i,t_n}(\mu)\mathbf{h}\right)}{\partial\theta_a} &= \frac{\partial\left(\boldsymbol{\lambda}_{s_i,t_n}(\mu)\mathbf{h}\right)}{\partial h_R[l]} = \boldsymbol{\lambda}_{s_i,t_n}(\mu)\frac{\partial\mathbf{h}}{\partial h_R[l]} \\ &= \bar{\lambda}_{s_i,t_n}(l,\mu)\end{aligned} \tag{38}$$

where $l = a-1$. Similarly, for $Q+1 \le a \le 2Q$

$$\begin{aligned}\frac{\partial\left(\boldsymbol{\lambda}_{s_i,t_n}(\mu)\mathbf{h}\right)}{\partial\theta_a} &= \frac{\partial\left(\boldsymbol{\lambda}_{s_i,t_n}(\mu)\mathbf{h}\right)}{\partial h_I[l]} = \boldsymbol{\lambda}_{s_i,t_n}(\mu)\frac{\partial\mathbf{h}}{\partial h_I[l]} \\ &= \jmath\bar{\lambda}_{s_i,t_n}(l,\mu)\end{aligned} \tag{39}$$

where $l = a-(Q+1)$. Therefore, it is straightforward to deduce that

$$\frac{\partial\left(\boldsymbol{\lambda}_{s_i,t_n}(\mu)\mathbf{h}\right)}{\partial h_I[l]} = \jmath\frac{\partial\left(\boldsymbol{\lambda}_{s_i,t_n}(\mu)\mathbf{h}\right)}{\partial h_R[l]}. \tag{40}$$

As a result, $\mathcal{I}(\boldsymbol{\theta})$ can be partitioned as[4]

$$\mathcal{I}(\boldsymbol{\theta}) = \begin{bmatrix}\mathcal{I}_{0,0} & \mathsf{Re}[\Upsilon] & -\mathsf{Im}[\Upsilon] \\ \mathsf{Re}[\Upsilon]^T & \mathsf{Re}[\Psi] & -\mathsf{Im}[\Psi] \\ -\mathsf{Im}[\Upsilon]^T & \mathsf{Im}[\Psi] & \mathsf{Re}[\Psi]\end{bmatrix} \tag{41}$$

where, based on (36)–(39)

$$\mathcal{I}_{0,0} = \frac{2}{\sigma_v^2}\mathsf{Re}\left[\sum_{i=0}^{S-1}\sum_{n=0}^{L-1}\left|\frac{\partial\left(\boldsymbol{\lambda}_{s_i,t_n}(\mu)\right)}{\partial\mu}\mathbf{h}\right|^2\right]. \tag{42}$$

Υ is a $1\times Q$ vector with its entries defined as

$$[\Upsilon]_{0,b} = \frac{2}{\sigma_v^2}\sum_{i=0}^{S-1}\sum_{n=0}^{L-1}\frac{\partial\left(\boldsymbol{\lambda}_{s_i,t_n}(\mu)\right)^*}{\partial\mu}\mathbf{h}^*\bar{\lambda}_{s_i,t_n}(b,\mu) \tag{43}$$

and Ψ is a $Q\times Q$ matrix defined as

$$[\Psi]_{a,b} = \frac{2}{\sigma_v^2}\sum_{i=0}^{S-1}\sum_{n=0}^{L-1}\left(\bar{\lambda}_{s_i,t_n}(a,\mu)\right)^*\bar{\lambda}_{s_i,t_n}(b,\mu). \tag{44}$$

The CRB on the covariance matrix of an unbiased estimator of $\boldsymbol{\theta}$, say $\hat{\boldsymbol{\theta}}$, is expressed as $\mathsf{Cov}(\hat{\boldsymbol{\theta}}) \ge \mathcal{I}(\boldsymbol{\theta})^{-1}$. In particular, we can obtain the CRB on the variance of an unbiased CFO estimator $\hat{\mu}$ as

$$\mathsf{Var}(\hat{\mu}) \ge \left[\mathcal{I}^{-1}(\boldsymbol{\theta})\right]_{0,0} = \mathrm{CRB}_\mu. \tag{45}$$

Note that in general, the entries of the vector Υ in (43) are not identically zero nor can they be neglected, and there is a coupling between the achievable estimation errors of μ and $\mathbf{h}$. As a result, the CRB on μ in the absence of channel knowledge will be larger than the one obtained with known

[4]To simplify notations, the dependence of the FIM entries on the parameter vector $\boldsymbol{\theta}$ is omitted

CIR, which would be simply $\mathcal{I}_{00}^{-1}$. Similarly, the lower bound on the variance of the CIR's lth tap is

$$\begin{aligned}\mathsf{Var}\left(\hat{h}[l]\right) &= \mathsf{Var}\left(\hat{h}_R[l]\right) + \mathsf{Var}\left(\hat{h}_I[l]\right) \\ &\geq \left[\mathcal{I}^{-1}(\boldsymbol{\theta})\right]_{l+1,l+1} + \left[\mathcal{I}^{-1}(\boldsymbol{\theta})\right]_{Q+l+1,Q+l+1} \\ &= \mathrm{CRB}_{h[l]}. \end{aligned} \tag{46}$$

Assuming independent estimates of the channel taps, we can obtain a lower bound on the average CIR estimation variance over the different taps by taking the average of (46), which can be expressed as

$$\mathrm{CRB}_{\mathbf{h}} = \frac{1}{Q}\left(\mathsf{tr}\left[\mathcal{I}^{-1}(\boldsymbol{\theta})\right] - \left[\mathcal{I}^{-1}(\boldsymbol{\theta})\right]_{0,0}\right). \tag{47}$$

This approach is convenient as it provides a single number against which to benchmark the performance of a particular channel estimation algorithm. Similar to what has been noted in [39] and [43], it can be seen that the CRB is a function of the particular channel realization. Note that in the above derivation of the CRB, we did not use the approximation given in (34) and factored in the contribution from all the input subbands as (13), although such simplifications as in Section III-B could also be applied.

V. Experimental Results

In this section, we investigate the performance of the proposed joint ML estimator of the CFO and CIR (30) and (31) through numerical simulations. The performance of the proposed estimator is compared with the derived CRB and some existing methods from the literature.

A. Methodology and Setup

We consider an OPRFB transceiver system (cf. Fig. 1) with burst of size $N = 60$ MCS, $M = 64$ subbands, $K = 72$ upsampling/downsampling factor, input sampling rate $F_s = 41.67$ kHz (equivalent to the channel bandwidth of $B = KF_s = 3$ MHz) and prototype filter of length $D = 24K$ designed as in [8]. The input data sequence $x_i[n]$ consists of independent and equiprobable 4-QAM symbols with normalized power to unity, i.e., $|x_i[n]| = 1$. Without loss in generality, since the pilot symbols are known to the receiver, we set $\mathsf{p}_{s_i}[t_n] = 1$ for all pair (s_i, t_n).

The data at the output of the transmit filter bank is passed through a frequency selective wireless channel with randomly generated coefficients $h[l]$, based on the International Telecommunication Union (ITU) Vehicular A channel guidelines [44]. The channel consists of 8 taps, where the fifth and seventh taps are set to zero and the other taps with delays 0, 0.33, 0.66, 1, 1.66, 2.33 microseconds obey a Rayleigh distribution with relative average powers of 0, -1, -9, -10, -15, -20 dB, respectively. Here, we consider two different channel models, i.e.,: time-invariant and time-varying. In the first case, the channel remains constant in time for the duration of a transmission burst while in the second case, the channel fading coefficients are correlated in time according to Jakes's model [45]. At the channel output, AWGN with power level of σ_ν^2 is added to the baseband received signal to obtain the desired SNR figure, defined as $\mathrm{SNR} = \sigma_s^2/\sigma_\nu^2$ with $\sigma_s^2 = E\{s[m]^2\}$ where $s[m] = \sum_{l=0}^{Q-1} h[l]y[M-1]$.

In our experiments, the proposed joint ML estimator of the CFO and CIR is implemented and compared to other possible approaches. In particular, based on the developed model for joint estimation in Section III-A, two separate ML estimators for the CFO and CIR alone (i.e., assuming that the other set of parameters is known *a priori*), and respectively denoted as MLE-CFO and MLE-CIR, are considered. Results are also provided for the ML-based CFO estimation method developed by the authors in [38], which assumes a flat fading AWGN channel with known gain and is referred to here as simplified ML estimator (SMLE). In addition to these various estimators, we show results for the CRBs on the minimum achievable estimator variance of the CFO and CIR, as derived in Section IV. Since the proposed joint estimator of the CFO and CIR has to estimate more unknown parameters, its performance is expected to be inferior to the separate estimation methods, i.e., MLE-CIR, MLE-CFO and SMLE, which make use of *a priori* knowledge and can therefore be considered as lower bounds on estimation error for comparison purposes.

Experiments are carried for different values of the system parameters, including: SNR, Doppler frequency, number of pilot-times and pilot-subbands; we also denote by μ_o the true value of the CFO. For each choice of parameter set, we run 10^3 independent Monte Carlo trials and compute the relevant performance measures under evaluation, i.e., the root mean squared error (RMSE) of the CFO and CIR estimates and the bit error rate (BER) of the OPRFB transceiver system with CFO compensation and CIR equalization derived from the corresponding estimator.[5] In particular, the CFO is compensated at the receiver front-end and the single-tap per subcarrier equalizer is used at the output of receiver to counteract the channel effects. The coefficients of this equalizer, e_i for $i \in \{0, \cdots M-1\}$, are obtained from the estimated CIR coefficients $\hat{h}[l]$ as

$$e_i = \left.\frac{1}{\hat{H}(z)}\right|_{z=w^i} \tag{48}$$

where $\hat{H}(z) = \sum_{l=0}^{Q-1} \hat{h}[l]z^{-l}$.

B. Results and Discussions

We first investigate the performance of the proposed method under the assumption of a time-invariant channel, and then later consider the case of a time-varying channel.

We begin with preliminary results aimed at justifying certain assumptions and choices made in our work. In Fig. 3, we sketch the cross-channel interference $|\Gamma_{i,j}^{n,p}(\mu)|$ for different values of p and j when n and i are fixed. It is evident that only a few subbands surrounding the target subband (here $i = 16$) are contributing as interference sources; it is therefore justified to set $\beta = 2$ in (34). Also, to support the choice of optimization method, a particular realization of the LLF (28) is plotted as a function of μ in Fig. 4, where the true CFO $\mu_o = 5\%$ of

[5]For the separate estimation methods, we simply assume exact knowledge of the missing parameters.

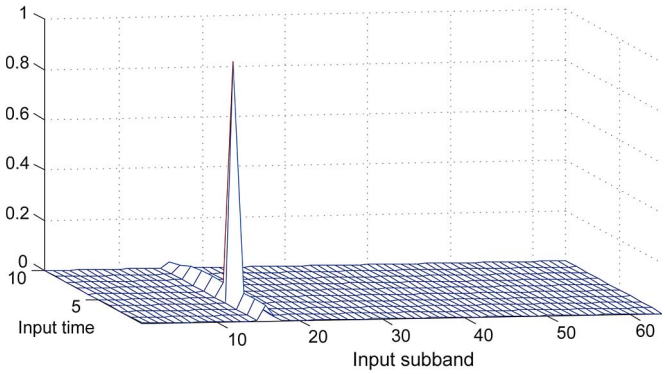

Fig. 3. Interference level $|\Gamma_{i,j}^{n,p}(\mu)|$ from pth input sample of jth subband on the nth output sample of ith subband ($p \in \{0, 1, \ldots, 10\}$, $j \in \{0, 1, \ldots, 63\}$, $n = 4$, $i = 16$, $\mu_o = 5\%$).

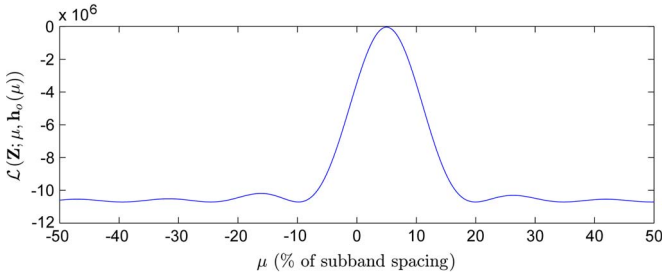

Fig. 4. Sample LLF versus CFO μ ($\mu_o = 5\%$, SNR $= 40$ dB, $S = 64$, $T = 6$, and $G = 1$).

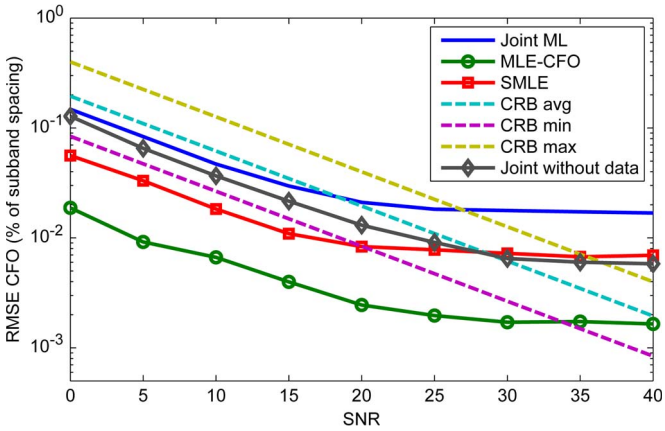

Fig. 5. RMSE of CFO estimation versus SNR ($\mu_o = 5\%$, $S = 64$, $T = 6$, and $G = 1$).

subband spacing. In general, we find that the LLF is convex in a wide region surrounding the true CFO.

Next, we investigate the performance of the proposed estimator as a function of the SNR, where the following parameter values are used: $\mu_o = 5\%$, $S = 64$, $T = 6$, and $G = 1$. Fig. 5 shows the RMSE performance of the CFO estimation for the proposed joint ML, MLE-CFO and SMLE methods, along with the CRB values as a function of SNR. To examine the effect of data-interference on the estimator accuracy, we also include results for the joint ML estimator when $w_{si}[t_n]$ (14) is set to zero (under *Joint without data*). As discussed in Section IV, the CRB is a function of the particular channel realization. Therefore, in Fig. 5, the average, minimum and maximum CRB over the different channel realizations are reported. Similarly, Fig. 6 shows the RMSE performance of the CIR estimation for

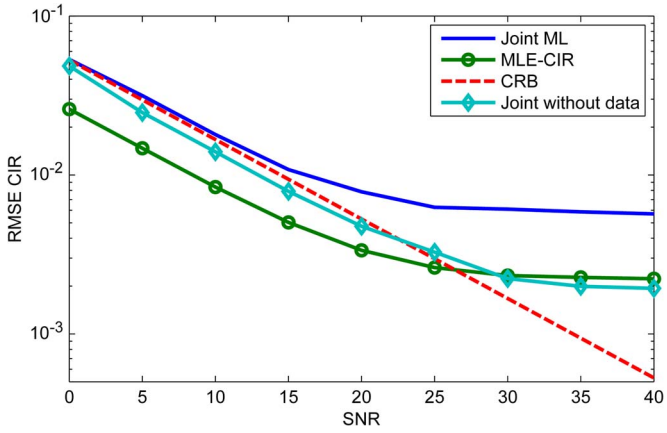

Fig. 6. RMSE of CIR estimation versus SNR ($\mu_o = 5\%$, $S = 64$, $T = 6$, and $G = 1$).

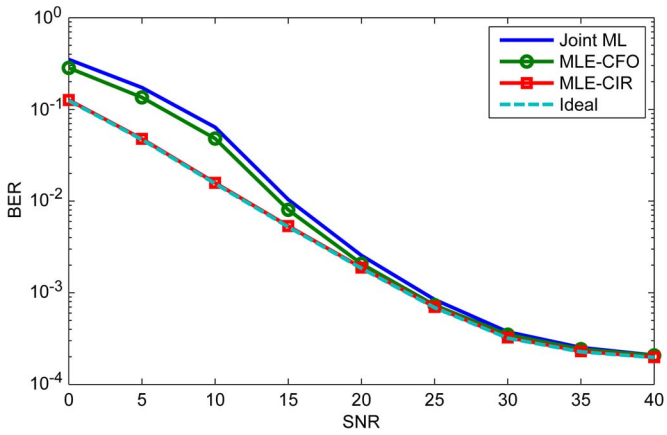

Fig. 7. BER versus SNR ($\mu_o = 5\%$, $S = 64$, $T = 6$, and $G = 1$).

the proposed joint ML (with and without data) and the MLE-CIR methods, along with the CRB. However, unlike Fig. 5 for CFO estimation, the dependency of the CRB on the channel realization is negligible in this case and, accordingly, we just report the average CRB.

It can be seen from Fig. 5 and 6 that at lower SNR, the proposed joint ML estimator provides an accuracy close to the (average) CRB for both the CFO and CIR parameters. Moreover, as expected, the MLE-CFO and MLE-CIR methods achieve the best performance since they benefit from exact knowledge of the CIR and CFO, respectively. Also, the MLE-CFO derived in this paper outperforms our previous SMLE method. At higher SNR, the estimation accuracy for all the methods reaches a lower floor due to several reasons. First, the simplifications made in Section III-B limit the accuracy of the estimator, whereas the CRB computation is exact. By increasing β in (34), we observed that the RMSE floor decreases at the cost of higher computational complexity. Another reason is due to the data noise term $w_{si}[t_n]$ in (14) which effectively limits the maximum achievable SNR to about 17 dB, consistent with the theoretical value computed from data-interference's power in (15). Finally, the accuracy of the estimator is limited by granularity of the search in the optimization process.

The BER performance of the OPRFB system employing single-tap per subcarrier equalizer and CFO compensation using the proposed joint ML, MLE-CFO and MLE-CIR is shown

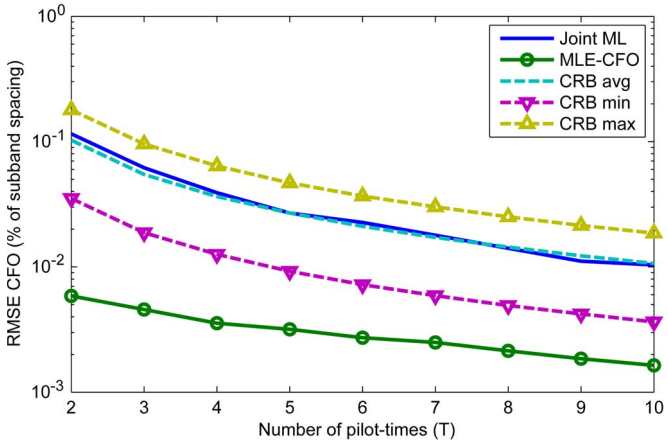

Fig. 8. RMSE of CFO estimation versus number of pilot-times ($\mu_o = 5\%$, $S = 64$, $G = 1$, and SNR $= 20$ dB).

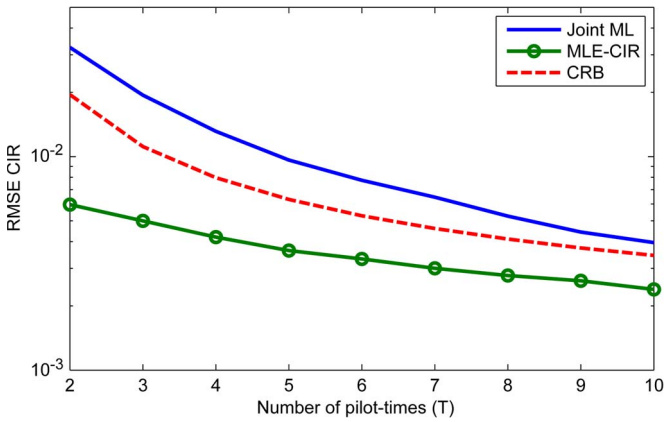

Fig. 9. RMSE of CIR estimation versus number of pilot-times ($\mu_o = 5\%$, $S = 64$, $G = 1$, and SNR $= 20$ dB).

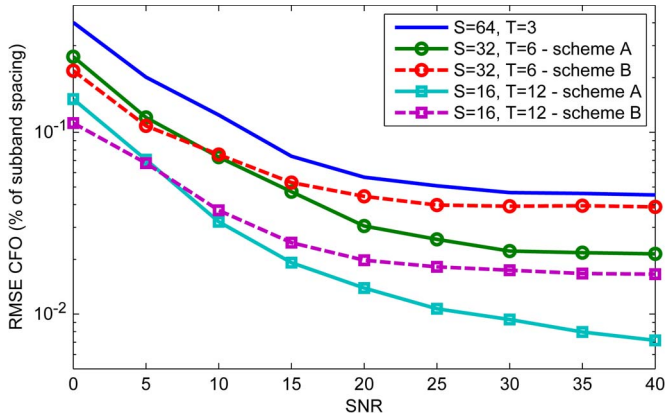

Fig. 10. RMSE of CFO estimation versus SNR for various pilot distributions in frequency ($\mu_o = 5\%$, $N_P = 192$, $G = 1$).

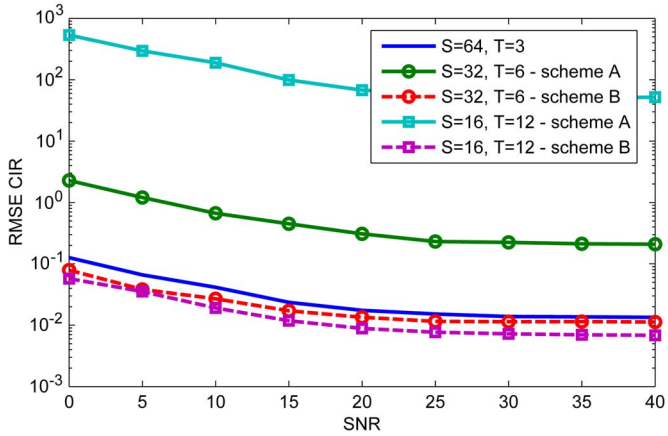

Fig. 11. RMSE of CIR estimation versus SNR for various pilot distributions in frequency ($\mu_o = 5\%$, $N_P = 192$, $G = 1$).

in Fig. 7, where the BER under ideal CFO and CIR knowledge is also provided as a benchmark. It can be seen that at high SNR, all of the proposed methods can reach the lower bound provided by ideal compensation, whereas the inaccuracy in CFO estimation at low SNR results in increased BER for the joint ML and MLE-CFO methods.

To clarify the tradeoff between estimation accuracy, on the one hand, and spectral efficiency and complexity, on the other hand, the RMSE performance of CFO and CIR estimation as a function of the total number of pilot-times T is presented in Figs. 8 and 9, respectively. These results show that the proposed method estimates the CFO with similar accuracy as the average CRB, whereas the CIR estimation performance remains slightly above the CRB. It can also be noted that the reduction in RMSE by increasing T is lower for larger values of T, which is typical of a the $1/T$ behavior in parameter estimation. Similar results (not reported here) are observed by increasing the number of pilot-subbands S with fixed T.

Next, we compare the RMSE performance of the proposed estimator with different distributions of pilots in frequency when the total number of pilots N_P is fixed. In particular, Figs. 10 and 11 show the RMSE performance of the CFO and CIR estimation as a function of SNR, respectively. It can be observed that in terms of CFO estimation accuracy, scheme A exhibits a superior performance compared to scheme B, due to the reduced effect of the data interference. However, as the pilots in scheme A are not scattered over the whole frequency band, this scheme is not capable of properly estimating the entire channel. Apart from the results associated to CIR estimation with scheme A, it can be seen that smaller values of S (and larger T) result in a higher estimation accuracy.

Alternatively, the RMSE performance of the proposed joint CFO and CIR estimator with different distributions of pilots in time is shown in Figs. 12 and 13, respectively. In particular, pilots are divided to $G = 1, 2$ and 3 groups and the estimator provides G different estimates of CIR corresponding to each group of pilots, whereas the CFO is assumed to be fixed over time. In this scenario with time-invariant channel model, the preamble implementation of the pilots (i.e., $G = 1$) displays a more accurate estimation of CFO and CIR compared to the case where $G = 2$ or $G = 3$. This superior performance is due to the fact that the data-interference is less when G is smaller.

In the wireless communication, when at least one side of the transmission (transmitter or receiver) is mobile, a Doppler shift spreads the signal in frequency and results in time-variation of the CIR. In Figs. 14 and 15, the RMSE performance of the proposed joint CFO and CIR estimation method for various distributions of pilots in time is plotted as a function of the maximum Doppler frequency f_D. The maximum Doppler

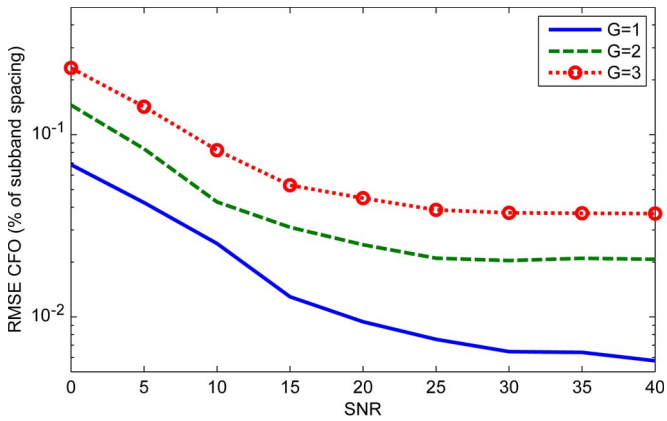

Fig. 12. RMSE of CFO estimation versus SNR for various pilot distributions in time ($\mu_o = 5\%$, $S = 64$, $T = 12$).

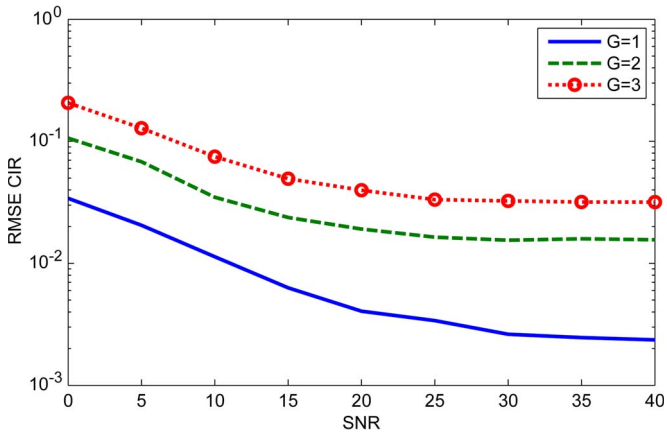

Fig. 13. RMSE of CIR estimation versus SNR for various pilot distributions in time ($\mu_o = 5\%$, $S = 64$, $T = 12$).

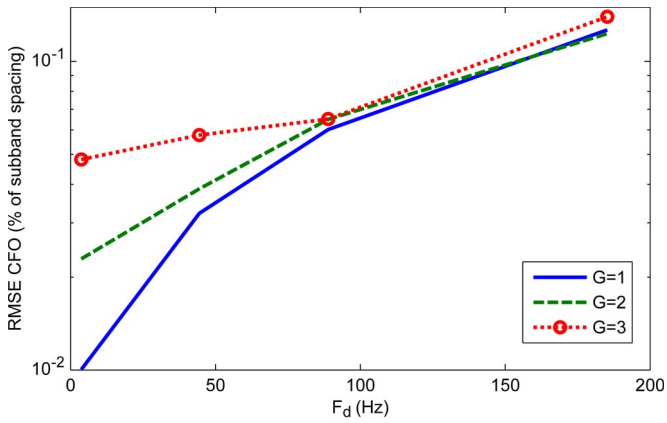

Fig. 14. RMSE of CFO estimation versus Doppler Frequency ($\mu_o = 5\%$, $S = 64$, $T = 12$, and SNR $= 20$ dB).

frequency can be derived as $f_D = vf_c/c_0$, where v is the mobile speed in m/s, f_c is the carrier frequency and $c_0 = 3 \times 10^8$ m/s is the speed of light. Here, we assume $f_c = 800$ MHz (similar to LTE and GSM). The values of f_D in Figs. 14 and 15, are equivalent to 4 different mobile speeds, that is 5, 60, 120 and 250 km/h corresponding to the speed of pedestrian, car in the urban area, car in the highway and high-speed train, respectively. The comparisons between these patterns show that for low mobility, CFO can be better estimated by the preamble

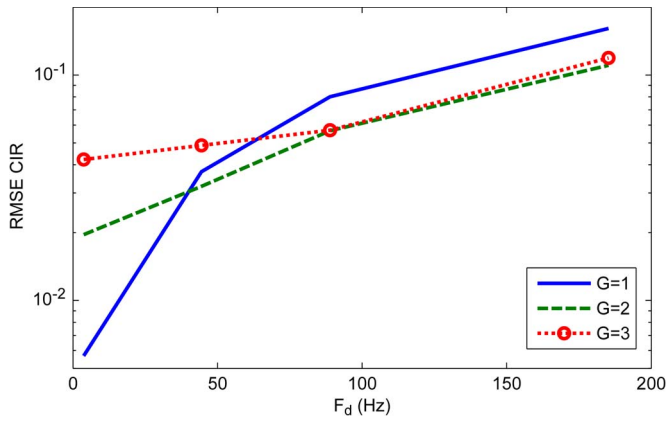

Fig. 15. RMSE of CIR estimation versus Doppler Frequency ($\mu_o = 5\%$, $S = 64$, $T = 12$, and SNR $= 20$ dB).

implementation of the pilots. However, with increased mobility, the difference between the CFO estimation accuracy with $G = 1, 2$ and 3 is negligible, whereas the scattered pilot schemes, i.e., $G = 2$ or 3, estimate the CIR slightly better than the preamble implementation of the pilots.

VI. Conclusion

In this paper, we proposed a data-aided joint ML estimator of CFO and CIR for OPRFB transceivers, where its complexity was considerably reduced through simplifying the underlying LLF. The CRB on the joint estimator variance was also derived and used as a benchmark. Moreover, different distributions of pilots over time-frequency plane were considered and tested for various scenarios over time-invariant and time-varying frequency selective channels. Simulation results demonstrated that the proposed estimator exhibits a performance close to the CRB and can robustly estimate CFO and CIR over different experimental setups. The development of a joint time offset estimator (along with the CFO and CIR) and a more extensive study of synchronization of OPRFB over time-varying channels can be seen as an interesting avenues to explore in the future.

Appendix A
Subband Noise

Due to the PR property imposed on $f_i[n]$ in (2), the covariance of the zero-mean term $\nu_i[n]$(10) can be written as

$$\begin{aligned}
&E\left\{\nu_i[p]\nu_j^*[r]\right\}\\
&=E\left\{\sum_{q_1=-\infty}^{\infty}\nu[q_1]f_i^*[q_1-pK]\sum_{q_2=-\infty}^{\infty}\nu^*[q_2]f_j[q_2-rK]\right\}\\
&=\sum_{q_1=-\infty}^{\infty}\sum_{q_2=-\infty}^{\infty}E\left\{\nu[q_1]\nu^*[q_2]\right\}f_i^*[q_1-pK]f_j[q_2-rK]\\
&=\sum_{q_1=-\infty}^{\infty}\sum_{q_2=-\infty}^{\infty}\delta_{q_1q_2}\sigma_\nu^2 f_i^*[q_1-pK]f_j[q_2-rK]\\
&=\sigma_\nu^2\sum_{q=-\infty}^{\infty}f_i^*[q-pK]f_j[q-rK]\\
&=\delta_{ij}\delta_{pr}\sigma_\nu^2. \qquad (49)
\end{aligned}$$

APPENDIX B
STATISTICAL PROPERTIES OF DATA-INTERFERENCE

Considering the input signal as an independent zero-mean random data sequence with variance σ_x^2 and based on the central limit theorem, we can model $w_{s_i}[t_n]$ as a zero-mean Gaussian random signal with

$$E\left\{w_{s_i}[t_n]w^*_{s_{i'}}[t_{n'}]\right\} = \sigma_x^2 \sum_{j\notin\mathcal{S}}\sum_{p\notin\mathcal{T}} \Gamma^{j,p}_{s_i,t_n}(\mu)\left(\Gamma^{j,p}_{s_{i'},t_{n'}}(\mu)\right)^* \tag{50}$$

where $\Gamma^{j,p}_{s_i,t_n}(\mu) = \sum_{l=0}^{Q-1}\gamma^{j,p}_{s_i,t_n}(l,\mu)h[l]$. When $s_i \neq s_{i'}$, due to excellent frequency selectivity of the prototype filters and similar to the simplification in (34), we can write that either $\Gamma^{j,p}_{s_i,t_n}(\mu) \simeq 0$ or $\Gamma^{j,p}_{s_{i'},t_n}(\mu) \simeq 0$ for $j \notin \mathcal{S}$. As a result, (50) can be approximated

$$E\left\{w_{s_i}[t_n]w^*_{s_{i'}}[t_{n'}]\right\} \simeq \delta_{s_i s_{i'}}\sigma_x^2 \sum_{j\notin\mathcal{S}}\sum_{p\notin\mathcal{T}} \Gamma^{j,p}_{s_i,t_n}(\mu) \times \left(\Gamma^{j,p}_{s_i,t_{n'}}(\mu)\right)^*. \tag{51}$$

Similarly, when $t_n \neq t_{n'}$, either $|p-t_n| \geq 2$ or $|p-t_{n'}| \geq 2$ for $p \notin \mathcal{T}$ in any implemented scheme of pilot distributions in time. As a result, for small values of μ and based on the PR property of the system, we can deduce that either $\Gamma^{j,p}_{s_i,t_n}(\mu) \simeq 0$ or $\Gamma^{j,p}_{s_i,t_{n'}}(\mu) \simeq 0$ for $p \notin \mathcal{T}$. Therefore, we can write

$$E\left\{w_{s_i}[t_n]w^*_{s_{i'}}[t_{n'}]\right\} \simeq \delta_{s_i s_{i'}}\delta_{t_n t_{n'}}\sigma_w^2 \tag{52}$$

where σ_w^2 is the variance of $w_{si}[t_n]$

$$\sigma_w^2 = E\left\{|w_{s_i}[t_n]|^2\right\} = \sigma_x^2 \sum_{p\notin\mathcal{T}}\sum_{j\notin\mathcal{S}} \left|\Gamma^{j,p}_{s_i,t_n}(\mu)\right|^2. \tag{53}$$

REFERENCES

[1] R. Van Nee and R. Prasad, *OFDM for Wireless Multimedia Communications*. Norwood, MA, USA: Artech House, 2000.

[2] L. Hanzo, Y. Akhtman, L. Wang, and M. Jiang, *OFDM for Wireless Multimedia Communications*. Hoboken, NJ, USA: Wiley, 2011.

[3] P. Siohan, C. Siclet, and N. Lacaille, "Analysis and design of OFDM/OQAM systems based on filterbank theory," *IEEE Trans. Signal Process.*, vol. 50, no. 5, pp. 1170–1183, May 2002.

[4] G. Cherubini, E. Eleftheriou, and S. Olcer, "Filtered multitone modulation for very high-speed digital subscriber lines," *IEEE J. Sel. Areas Commun.*, vol. 20, no. 5, pp. 1016–1028, Jun. 2002.

[5] C. Siclet, P. Siohan, and D. Pinchon, "Perfect reconstruction conditions and design of oversampled DFT-modulated transmultiplexers," *EURASIP J. Appl. Signal Process.*, vol. 2006, pp. 15756-1–15756-14, Jan. 2006.

[6] F. Duplessis-Beaulieu and B. Champagne, "Design of prototype filters for perfect reconstruction DFT filter bank transceivers," *Signal Process.*, vol. 89, no. 1, pp. 87–98, Jan. 2009.

[7] S. Rahimi and B. Champagne, "Perfect reconstruction DFT modulated oversampled filter bank transceivers," in *Proc. Eur. Signal Process. Conf.*, Barcelona, Spain, Aug. 2011, pp. 1588–1592.

[8] S. Rahimi and B. Champagne, "Oversampled perfect reconstruction DFT modulated filter banks for multi-carrier transceiver systems," *Signal Process.*, vol. 93, no. 11, pp. 2942–2955, Nov. 2013.

[9] B. Farhang-Boroujeny, "OFDM versus filter bank multicarrier," *IEEE Signal Process. Mag.*, vol. 28, no. 3, pp. 92–112, May 2011.

[10] M. Renfors, P. Siohan, B. Farhang-Boroujeny, and F. Bader, "Filter banks for next generation multicarrier wireless communications," *EURASIP J. Adv. Signal Process.*, vol. 2010, pp. 314193-1–314193-2, May 2010.

[11] D. M. Arndt and C. A. F. da Rocha, "Performance comparison between OFDM and FBMC systems in digital TV transmission," in *Proc. IEEE Latin-Amer. Conf. Commun.*, Oct. 2011, pp. 1–6.

[12] B. Farhang-Boroujeny, "Filter bank spectrum sensing for cognitive radios," *IEEE Trans. Signal Process.*, vol. 56, no. 5, pp. 1801–1811, May 2008.

[13] S. Baig and M. J. Mughal, "Multirate signal processing techniques for high-speed communication over power lines," *IEEE Commun. Mag.*, vol. 47, no. 1, pp. 70–76, Jan. 2009.

[14] T. Wang, J. G. Proakis, and J. R. Zeidler, "Interference analysis of filtered multitone modulation over time-varying frequency-selective fading channels," *IEEE Trans. Commun.*, vol. 55, no. 4, pp. 717–727, Apr. 2007.

[15] A. M. Tonello and F. Pecile, "Analytical results about the robustness of FMT modulation with several prototype pulses in time-frequency selective fading channels," *IEEE Trans. Wireless Commun.*, vol. 7, no. 5, pp. 1634–1645, May 2008.

[16] T. H. Stitz, T. Ihalainen, A. Viholainen, and M. Renfors, "Pilot-based synchronization and equalization in filter bank multicarrier communications," *EURASIP J. Adv. Signal Process.*, vol. 2010, pp. 1–18, Jan. 2010.

[17] P. K. Remvik, N. Holte, and A. Vahlin, "Fading and carrier frequency offset robustness for different pulse shaping filters in OFDM," in *Proc. IEEE Veh. Technol. Conf.*, May 1998, vol. 2, pp. 777–781.

[18] T. Pollet, M. Van Bladel, and M. Moeneclaey, "BER sensitivity of OFDM systems to carrier frequency offset and Wiener phase noise," *IEEE Trans. Commun.*, vol. 43, no. 2–4, pp. 191–193, Feb.–Apr. 1995.

[19] T. Bianchi, F. Argenti, and E. DelRe, "Performance of filterbank and wavelet transceivers in the presence of carrier frequency offset," *IEEE Trans. Commun.*, vol. 53, no. 8, pp. 1323–1332, Aug. 2005.

[20] T. Fusco, A. Petrella, and M. Tanda, "Sensitivity of multi-user filterbank multicarrier systems to synchronization errors," in *Proc. Int. Symp. Commun., Control, Signal Process.*, Mar. 2008, pp. 393–398.

[21] H. Saeedi-Sourck, Y. Wu, J. W. Bergmans, S. Sadri, and B. Farhang-Boroujeny, "Sensitivity analysis of offset QAM multicarrier systems to residual carrier frequency and timing offsets," *Signal Process.*, vol. 91, no. 7, pp. 1604–1612, Jul. 2011.

[22] S. Rahimi and B. Champagne, "On the robustness of oversampled filter bank multi carrier systems against frequency offset," in *Proc. Int. Symp. Wireless Commun. Syst.*, Aug. 2012, pp. 944–948.

[23] P. Moose, "A technique for orthogonal frequency division multiplexing frequency offset correction," *IEEE Trans. Commun.*, vol. 42, no. 10, pp. 2908–2914, Oct. 1994.

[24] J. van de Beek, M. Sandell, and P. Borjesson, "ML estimation of time and frequency offset in OFDM systems," *IEEE Trans. Signal Process.*, vol. 45, no. 7, pp. 1800–1805, Jul. 1997.

[25] X. Ma, H. Kobayashi, and S. Schwartz, "Joint frequency offset and channel estimation for OFDM," in *Proc. IEEE Global Telecommun. Conf.*, Dec. 2003, vol. 1, pp. 15–19.

[26] J.-H. Lee, J. C. Han, and S. C. Kim, "Joint carrier frequency synchronization and channel estimation for OFDM systems via the EM algorithm," *IEEE Trans. Veh. Technol.*, vol. 55, no. 1, pp. 167–172, Jan. 2006.

[27] T. Fusco, A. Petrella, and M. Tanda, "Data-aided symbol timing and CFO synchronization for filter bank multicarrier systems," *IEEE Trans. Wireless Commun.*, vol. 8, no. 5, pp. 2705–2715, May 2009.

[28] D. Mattera and M. Tanda, "Data-aided synchronization for OFDM/OQAM systems," *Signal Process.*, vol. 92, no. 9, pp. 2284–2292, Sep. 2012.

[29] E. Kofidis, D. Katselis, A. Rontogiannis, and S. Theodoridis, "Preamble-based channel estimation in OFDM/OQAM systems: A review," *Signal Process.*, vol. 93, no. 7, pp. 2038–2054, Jul. 2013.

[30] P. Amini and B. Farhang-Boroujeny, "Packet format design and decision directed tracking methods for filter bank multicarrier systems," *EURASIP J. Adv. Signal Process.*, vol. 2010, pp. 307 983-1–307 983-13, 2010.

[31] H. Saeedi-Sourck, S. Sadri, Y. Wu, and B. Farhang-Boroujeny, "Near maximum likelihood synchronization for filter bank multicarrier systems," *IEEE Wireless Commun. Lett.*, vol. 2, no. 2, pp. 235–238, Apr. 2013.

[32] A. Tonello and F. Rossi, "Synchronization and channel estimation for filtered multitone modulation," in *Proc. Int. Symp. Wireless Pers. Multim. Commun.*, Sep. 2004, pp. 590–594.

[33] M. Carta, V. Lottici, and R. Reggiannini, "Frequency recovery for filterbank multicarrier transmission on doubly-selective fading channels," in *Proc. IEEE Int. Conf. Commun.*, Jun. 2007, pp. 5212–5217.

[34] V. Lottici, R. Reggiannini, and M. Carta, "Pilot-aided carrier frequency estimation for filter-bank multicarrier wireless communications on doubly-selective channels," *IEEE Trans. Signal Process.*, vol. 58, no. 5, pp. 2783–2794, May 2010.

[35] V. Lottici, M. Luise, C. Saccomando, and F. Spalla, "Blind carrier frequency tracking for filterbank multicarrier wireless communications," *IEEE Trans. Commun.*, vol. 53, no. 10, pp. 1762–1772, Oct. 2005.
[36] T. Fusco, A. Petrella, and M. Tanda, "Blind CFO estimation for noncritically sampled FMT systems," *IEEE Trans. Signal Process.*, vol. 56, no. 6, pp. 2603–2608, Jun. 2008.
[37] M. Bellanger *et al.*, "FBMC Physical Layer: A Primer," PHYDYAS, Paris , France, Jan. 2010.
[38] S. Rahimi and B. Champagne, "Carrier frequency recovery for oversampled perfect reconstruction filter bank transceivers," in *Proc. Int. Conf. Wireless Mobile Commun.*, Jul. 2013, pp. 140–145.
[39] M. Morelli and U. Mengali, "Carrier-frequency estimation for transmissions over selective channels," *IEEE Trans. Commun.*, vol. 48, no. 9, pp. 1580–1589, Sep. 2000.
[40] F. Duplessis-Beaulieu and B. Champagne, "One-tap equalizer for perfect reconstruction DFT filter bank transceivers," in *Proc. Int. Symp. Signals, Syst. Electron.*, Aug. 2007, pp. 391–394.
[41] S. Kay, *Fundamentals of Statistical Signal Processing, Vol. I: Estimation Theory*. Upper Saddle River, NJ, USA: Prentice-Hall, 1993.
[42] H. Arslan and T. Yucek, "Delay spread estimation for wireless communication systems," in *Proc. IEEE Int. Sym. Comput. Commun.*, Jun. 2003, pp. 282–287.
[43] P. Stoica and O. Besson, "Training sequence design for frequency offset and frequency-selective channel estimation," *IEEE Trans. Commun.*, vol. 51, no. 11, pp. 1910–1917, Nov. 2003.
[44] *Guidelines for Evaluation of Radio Transmission Technologies for IMT-2000*, Recommendation ITU-R M. 1225, 1997.
[45] W. Jakes, *Microwave Mobile Communications*. Piscataway, NJ, USA: IEEE Press, 1994.

Siavash Rahimi (S'01) received the B.S. degree from the University of Tehran, Tehran, Iran, in 2005, the M.S. degree from Concordia University, Montreal, QC, Canada, in 2008, and the Ph.D. degree from McGill University, Montreal, in 2014, all in electrical engineering. His research interests include multi-rate signal processing, parameter estimation, multiple access techniques, and applications thereof to wireless telecommunication networks. Mr. Rahimi was a recipient of several awards and scholarships, including FQRNT Doctoral Research Scholarship, McGill Engineering Doctoral Award, and Les Vadasz Engineering Fellowship, among others. In 2007, he was a System Engineer with Nortel Networks, Ottawa, ON, Canada, where he implemented a pre-congestion control mechanism for an IETF standard. He is currently a Senior Consultant for Strategy& (formerly Booz & Company), where he focuses on the energy and telecommunication industries.

Benoit Champagne (S'87–M'89–SM'03) received the B.Ing. degree in engineering physics from the Ecole Polytechnique de Montréal, Montreal, QC, Canada, in 1983, the M.Sc. degree in Physics from the Université de Montréal, Montreal, in 1985, and the Ph.D. degree in electrical engineering from the University of Toronto, Toronto, ON, Canada, in 1990.

From 1990 to 1999, he was an Assistant and then Associate Professor at INRS-Telecommunications, Université du Quebec, Montreal. In 1999, he joined McGill University, Montreal, where he is now a Full Professor within the Department of Electrical and Computer Engineering. He served as Associate Chairman of Graduate Studies in the Department from 2004 to 2007. His research focuses on the study of advanced algorithms for the processing of information bearing signals by digital means. His interests span many areas of statistical signal processing, including detection and estimation, sensor array processing, adaptive filtering, and applications thereof to broadband communications and audio processing, where he has coauthored nearly 200 referred publications. His research has been funded by the Natural Sciences and Engineering Research Council (NSERC) of Canada, the "Fonds de Recherche sur la Nature et les Technologies" from the Government of Quebec, as well as some major industrial sponsors, including Nortel Networks, Bell Canada, InterDigital, and Microsemi. He has been an Associate Editor for the IEEE SIGNAL PROCESSING LETTERS, the IEEE TRANSACTIONS ON SIGNAL PROCESSING, and the *EURASIP Journal on Applied Signal Processing*. He has also served on the Technical Committees of several international conferences in the fields of communications and signal processing. In particular, he was Co-Chair, Wide Area Cellular Communications Track, for the IEEE International Symposium on Personal, Indoor and Mobile Radio Communications (Toronto, ON, Canada, September 2011); Co-Chair, Antenna and Propagation Track, for the IEEE Vehicular Technology Conference-Fall (Los Angeles, CA, USA, September 2004); and Registration Chair for the IEEE International Conference on Acoustics, Speech and Signal Processing (Montreal, QC, Canada, May 2004).